Additive Manufacturing 50 (2022) 102572

Contents lists available at ScienceDirect

Additive Manufacturing

journal homepage: www.elsevier.com/locate/addma

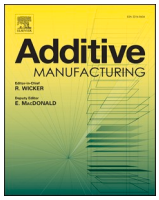

Research paper

Laser incidence angle influence on energy density variations, surface roughness, and porosity of additively manufactured parts

Parvin Fathi-Hafshejani [a,c], Arash Soltani-Tehrani [b,c], Nima Shamsaei [b,c], Masoud Mahjouri-Samani [a,c,*]

[a] Department of Electrical and Computer Engineering, Auburn University, Auburn, AL, USA
[b] Department of Mechanical Engineering, Auburn University, Auburn, AL, USA
[c] National Center for Additive Manufacturing Excellence (NCAME), Auburn University, Auburn, AL, USA

ARTICLE INFO

Keywords:
Laser beam powder bed fusion (LB-PBF/L-PBF)
Laser incidence angle
Laser beam elongation
Melt pool size variation
Energy density variation

ABSTRACT

The use of additive manufacturing (AM) technologies for fabricating structural and functional parts is rapidly rising due to their transformative design flexibility and customizability. However, maintaining the uniformity and consistency of the fabricated part across the build plate is a critical challenge. One of the main sources of variability across the build plate is laser spot elongation in laser beam powder bed fusion (LB-PBF) AM which typically occurs when the beam moves from the center of the plate to the edge at different incidence angles. This laser spot elongation may then result in the loss of laser power density which can potentially cause elongated melt pools, poor dimensional accuracy, and formation of lack of fusion and more gas entrapped pores in the final part. Here, we report both geometrical calculations and experimental evidence to show the behavior of the laser in the different areas of the build plate. A pulsed laser is first used to show and calculate the geometrical footprint of the beam elongations at different incidence angles. Then, the surface roughness, melt pool size, and porosity variations are investigated for varying laser interaction cross-section across the build plate by manufacturing AlSi10Mg (an aluminum alloy) parts and correlating them to theoretical calculations. It is found that for given optimized process parameters at the center of the build plate, as the beam goes farther away from the center, it becomes elongated. As the power density falls, melt pool width becomes wider, melt pool depth becomes shallower (depending on the elongation orientation with respect to the scan direction), and the number of lack of fusion defects increases. This work provides fundamental insight into possible sources of variations across the build plate in an LB-PBF process that may help design new strategies to compensate for such variations to enhance uniformity and reliability of AM parts.

1. Introduction

The application of lasers has been vastly growing in various sectors, including additive manufacturing (AM), healthcare, aerospace, and automotive industries due to their high efficiency, high temporal and spatial precision, controlled power and energy densities, as well as compatibility with automation and artificial intelligence (AI) [1,2]. For instance, in the manufacturing sector, nowadays, it is easy to find a large number of research areas on laser technologies, including melting [3,4], cutting [5,6], welding [7,8], cladding [9,10], coating [2,11] and additive technologies [12–14]. Among these technologies, laser-based AM processes such as laser beam powder bed fusion (LB-PBF) [15–22] is one of the fastest-growing methods transforming the way parts are being manufactured. To build comparable or better parts than their conventional counterparts, it is crucial to fully understand and control the fundamental mechanisms involved in the AM process. From the laser point of view, understanding the lasers, optics, and laser-powder interactions is essential in order to decipher the possible sources of variations in the process. This allows for designing strategies and techniques in order to eliminate or compensate for such variations and enhance the uniformity, quality, reliability, and reproducibility of the printed parts [23,24].

For instance, the laser interplay with the powder is considered one of the most critical factors in LB-PBF printing [24,25]. The laser's interaction with powder is a complex phenomenon that occurs on fast time and microscopic size scales, often on the focal plane of the laser beam

* Corresponding author at: Department of Electrical and Computer Engineering, Auburn University, Auburn, AL, USA.
E-mail address: Mahjouri@auburn.edu (M. Mahjouri-Samani).

https://doi.org/10.1016/j.addma.2021.102572
Received 12 October 2021; Received in revised form 14 December 2021; Accepted 17 December 2021
Available online 22 December 2021

with optimal power density for melting and sintering processes. Running on these small temporal and spatial scales suggests that even minor deviations from the optimal processing parameters can significantly impact the structural and mechanical properties of the final manufactured parts [26–33]. The location of the parts on the build plate is one of the sources of deviation in the LB-PBF process [23,34–36]. One contributing factor is the effect of beam incidence angle which results in beam elongation at high deflection angles, especially at the edge of the build plate, as presented in Fig. 1. This beam elongation increases the beam cross-sectional area, which varies depending on the location of the part on the build plate, potentially resulting in a considerable power density loss (i.e., W/cm^2). If the process parameters are optimized for the center of the build plate, then parts closer to the edge may suffer from the lack of adequate power density which can form additional lack of fusion defects in the material. On the other hand, if the process parameters are optimized for the edge of the build plate, then parts closed to the center may suffer from excessive power density, which can potentially form keyhole defects. Fig. 2.

Recently, some studies also reported surface roughness variations in the LB-PBF parts depending on the laser incidence angle [34,37,38]. They attributed this behavior to the varying laser spot size in different locations, influencing the melt pool shape and stability. The interdependent effects of the laser incidence angle and surface orientation on the surface roughness of the LB-PBF parts is also studied by others [38,39]. To analyze this interdependency, the concept of surface laser relation angle ζ was introduced in [38]. Based on this parameter, they re-designed the entire build plate geometry to decrease the laser incidence polar angle and improve the part roughness quality. However, most research activities only have focused on the incidence angle and the impact of elongation on volumetric defects and surface roughness. No fundamental research has been so far conducted on why and how these changes occur. This study will tackle the problem from the perspective of the laser-materials interaction (i.e., power density, energy density, and interaction time) and explain how the incidence angle can change these parameters. A comprehensive study is done to show the beam projection and how it affects the microstructure, melt pool geometry, and the quality of final parts. Finally, it is shown how the specimen orientation can reduce the impact of incidence angle and improve the quality of final parts.

2. Materials and methods

The effect of laser incidence angle on the laser footprint and melt pool geometry were studied by two different experimental designs, including i) single laser pulse experiment and ii) laser beam powder bed fusion (LB-PBF) experiment.

2.1. Single laser pulse experiment

The first experiment was designed with a nanosecond fiber laser (1064 nm wavelength with pulse widths ranging from 5 to 2000 ns, pulse energy ranging from 0.04 to 1.57 mJ, and a repetition rate ranging from 1 Hz to 4160 kHz) to precisely create and capture the laser footprint at different locations. The goal of this experiment was to show the variations in the laser interaction cross-section on different locations of the build plate (aluminum plate 25 ×25 cm^2) and how it changes the corresponding energy densities. For better clarity of the footprints, instead of using powder, we used an aluminum sheet for this experiment. A grid of 20 × 20 cm^2 uniformly dispersed spots was designed to test the entire workspace of the build plate. In this experiment, a single laser pulse with a power of 91 W and a pulse duration of 2020 ns was used to generate the laser interaction cross-section footprints.

2.2. LB-PBF experiment

The second experiment was designed to investigate the effects of the laser incidence angle on parts manufactured by LB-PBF technology. Fig. 1 shows the schematics of the build layout printed in a Renishaw AM250, an LB-PBF machine, with argon as the shielding gas. Table 1 shows process parameters which is used to manufacture AlSi10Mg parts. To better observe the melt pool, the layer rotation was turned off during the print – i.e., laser passes are parallel to each other. Argon-atomized AlSi10Mg powder with an initial particle size distribution (PSD) of 15–45 μm from Carpenter Additive was used to manufacture these test parts. The powder chemical composition reported by the manufacturer is provided in Table 2. The geometrical analysis, roughness, and porosity levels were studied using a KEYENCE VHX-6000 digital microscope. It should also be mentioned that due to the scanner acceleration and deceleration at the beginning and end of the scanned line, typically machine manufacturers consider mitigation plans such as skywriting and homogenization to retreat these affected locations. In this study, to eliminate the contour effect, we removed the contour scan and focused our investigation on the inner portions away from the beginning and end of the tracks. This allowed us to purely focus on understanding the impact of laser incidence angle on melt pool geometry, roughness, and porosity of the parts.

3. Basic principles (theory/calculation)

A laser beam interaction with powder can be represented by power density, the time of irradiation, and the heat-affected zone size on the specimen. The average power density (P_d) is described as the ratio of the laser power (P) to the area of laser spot cross-section on the surface (A_S), which is given by [40]:

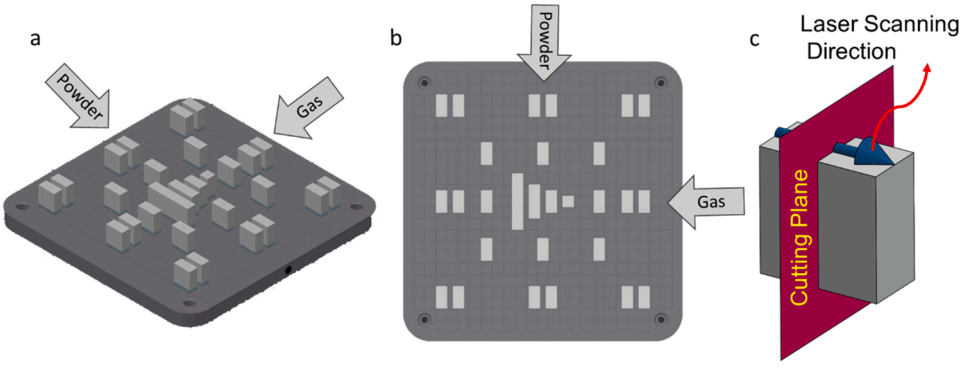

Fig. 1. Isometric (a) and top (b) views of the build layout used to fabricate the parts for studying the laser incidence angle and beam elongation effect. Illustration of the cutting plane and laser scanning direction on the specimen (c).

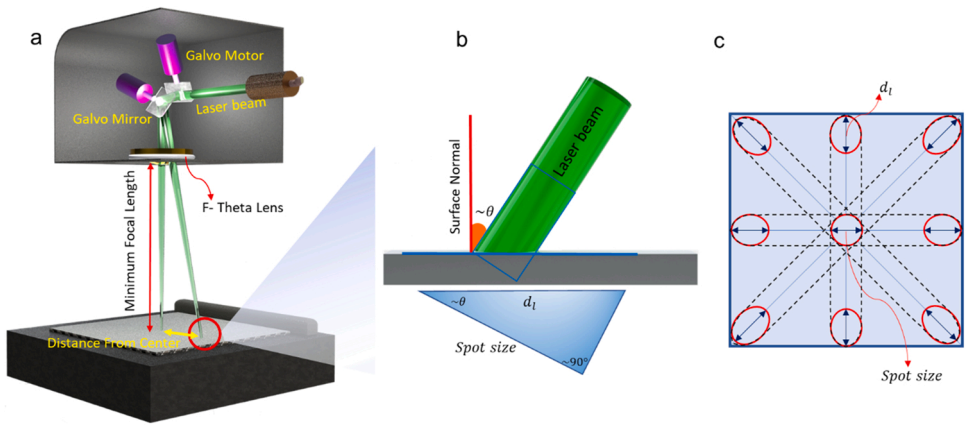

Fig. 2. Effects of laser incidence angle: Diagram of the LB-PBF process showing the scanner operation and the possible laser incidence angles on the build plate (a). The incidence angle effect on the interaction cross-section on the surface (b). Schematic representation of the laser beam elongation on various locations of the build plate (c).

Table 1
Process parameters for AlSi10Mg parts.

Power (W)	Point Distance (μm)	Exposure Time (μs)	Speed[a] (m/s)	Hatch Distance (μm)	Layer Thickness (μm)	Layer Rotation (°)
200	80	140	0.53	130	25	0

[a] $Speed = \frac{Point\ \ Distance}{(Exposure\ \ Time + 10)}$ (Provided by Renishaw)

Table 2
Chemical composition of the gas-atomized AlSi10Mg in weight percentage reported by the manufacturer.

Element	Al	Mn	O	Pb	Sn	Si	Mg	Zn	Ni	Fe	Ti	Cu	N
%Weight	balance	0.45	0.10	0.05	0.05	9–11	0.2–0.45	0.10	0.05	0.55	0.15	0.05	0.05

$$Power\ \ density\ \ (P_d) = \frac{Laser\ \ power\ \ (P)}{Area\ \ of\ \ laser\ \ spot\ \ (A_s)} \quad (1)$$

The time in which the laser beam exposes a particular point on the workpiece while the beam is moving at a constant speed is defined as the interaction time (t_i). Considering a center of a circular beam with a diameter (d) that travels on the surface with speed (v), the interaction time can then be given by Eq. (2). This definition describes the maximum interaction time in the beam centerline. In reality, the interaction time may diverge across the laser scan directions due to the variation in the beam circularity [41].

$$Interaction\ \ time\ \ (ti) = \frac{Laser\ \ spot\ \ diameter\ \ (d)}{Laser\ \ travel\ \ speed\ \ (v)} \quad (2)$$

For a laser beam with a constant interaction time and uniform intensity distribution (i.e., Gaussian in most cases) across the laser spot, the specific energy is given by Eq. (3) [41]:

$$Energy\ \ density = Power\ \ density(P_d) \times Interaction\ \ time\ \ (ti) \quad (3)$$

The laser incidence angle on the surface can result in an inconsistent beam profile and non-uniform beam shape during the manufacturing process. For example, changing the incidence angle from a normal incidence (i.e., 0°) to 20° can cause the power density to drop by 6% due to the beam elongation, while laser power and travel speed are kept constant. This happens due to beam elongation, which changes the beam from a circular to an elliptical shape and increases the interaction cross-section area. Fig. 2 shows the geometrical variation of the beam shape at various incidence angles on the build plate. When the beam size or shape changes while the laser power and scan speed are kept constant, the power and energy densities on the specimen also change, potentially resulting in structural and mechanical changes. This paper investigates the effect of such location-dependent beam shape, area, and energy variations on the quality of specimens [40,41].

4. Experimental results

4.1. Effect of laser incidence angle on the shape of the beam interaction cross-section on the build plate

The interaction cross-section of the laser beam on the build plate depends on the incidence angle and hence the beam distance from the center of the build plate, as shown in Fig. 3. A larger distance from the center results in more elliptical laser footprints. The incidence angle (θ) can be calculated by Eq. (4). The smaller diameter of the elliptical shape is equal to the laser spot diameter, and depending on the location of the beam on the build plate, the larger diameter (d_l) can be determined by Eq. (5). To experimentally verify such incidence angle-induced beam elongations footprints, we employed a pulsed nanosecond laser to precisely capture the laser footprints on the surface using a single pulse without extended time heat impacts. In addition, because of the pulsed laser, the interaction time and hence energy density only depends on power density for a single pulse. Therefore, the decreasing energy density can solely be attributed to the elongation effect. If the laser power is optimized to create a melt in the center of the build plate, then as the beam travels farther from the center, the energy density decreases and cannot melt the workpiece as sufficient as the center. Therefore, the laser footprint is smaller than the calculated diameter. However, the elliptical ratio (i.e., the ratio of the major axis to the minor axis) gets bigger, and the elliptical shape can be distinguished more as the distance becomes larger, as shown in Fig. 3.

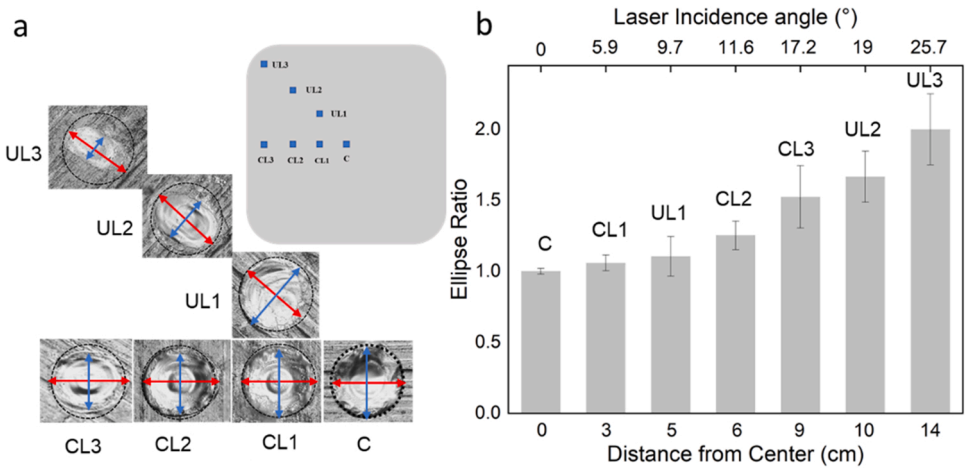

Fig. 3. Capturing the laser spot footprint at different locations on the build plate using a pulsed nanosecond laser. Optical images of the beam footprints were obtained from the labeled areas on the build plate (a). The corresponding aspect ratio along with the error bar of the elongated elliptical beams corresponding to the indicated location and incidence angle (b).

$$tan\quad \theta = \frac{\text{Distance from center}}{\text{Minimum focal length}} \tag{4}$$

$$d_l = \frac{Spotsize}{Cos\theta} \tag{5}$$

4.2. *Effect of laser incidence angle on the melt pool geometry and structure of the printed parts*

The second set of experiments was designed to investigate the impact of the angle of incidence on the melt pool geometry and structure of the specimens manufactured by the LB-PBF process. These specimens were specially designed to study their internal melt pool sizes and geometries as well as the quality of the parts at each condition. Specimens with rectangular geometries (2 cm length × 1 cm width × 2 cm height) were positioned on different locations of the build plate with a radial distance of 50, 65, 100, and 130 mm from the center, as shown in Fig. 4a. These specimens were printed in a Renishaw AM250, an LB-PBF machine, in an argon environment and using the factory suggested process parameters for AlSi10Mg (Table 1). This machine provides a laser beam diameter of 70 μm at the focal point on the surface of the build plate. To avoid melt pool distortion, the parts were fabricated without contours, and layers were printed with a constant scan strategy in each layer (i.e., no scan rotation from layer to layer). This allowed us to align the melt pools on each other for precise analysis and measurements.

All the parts were cut perpendicular to the laser tracks, mounted, and polished for melt pool studies. The planar grinding included five steps using sandpapers with grits ranging from 320 (grain size of 46.3 μm) to 4000 (grain size of 5 μm). Once the surface was ready, it was polished using colloidal silica of 0.05 μm. Once the mirror-like surface finish was achieved, surface images were taken using a Keyence VHX-6000 digital microscope with 100X magnification.

Fig. 4b,c,d shows the melt pool structures of three specimens as highlighted on the build plate (i.e., at the center and radial distances of 100 and 130 mm from the center). The part corresponding to the center shows a uniform pattern of laser tracks with the melted areas oriented in a vertical direction (Fig. 4b) since the beam is a circular Gaussian beam at the center represented by the circular black circle. When the distance from the center increases, the beam gets elongated at different angles depending on the location of the build plate, as represented by the red circles for each location. Hence, the melt pool patterns become distorted and elongated (see Fig. 4c, d). It should be noted that the laser tracks were not rotated in the layers, hence all layers were printed in parallel and on top of each other for better measurements and data analysis, as shown in Fig. 4b,c,d.

The melt pool geometry of the parts was measured to understand how changes in the laser interaction cross-section area, shape, power density, and energy density affect the melt pool while interaction time is constant. The measurement was done based on the NASA MSFC-SPEC-3717 document [42] and literature [43–45]. The widths of the melt

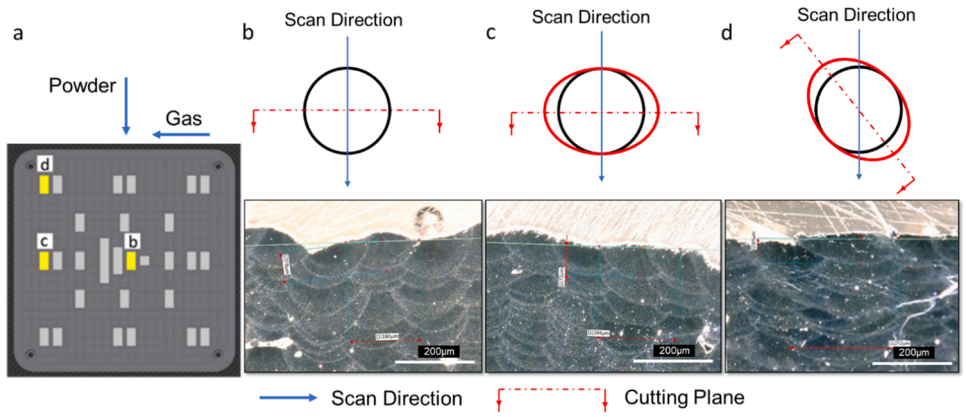

Fig. 4. Parts locations on the build plate designed for investigating the effect of incidence angle and beam elongation on the melt pool geometry and size (a). Optical image of the melt pool structures printed at different parts of the build plate as highlighted, including the central part (incidence angle 0°) (b), 100 mm away from the center (left) (incidence angle 14°) (c), and 130 mm away from the center (top left corner) (incidence angle 18°) (d).

pools were measured in three regions in the inner layers of the part, and their averages were calculated. Fig. 5a shows the inner layers and last layer widths of the printed parts at different incidence angles, indicating the same trend for both. The last layer melt pools are slightly wider, possibly because they have only melted once and are not affected by further layers. The last layers' melt pool depth of the parts at each location were also measured, as shown in Fig. 6b. The melt pool depth decreases moving farther away from the center because of the decreasing energy and power densities while the interaction time is almost constant. It should be noted that the inner layer melt pool depth was not considered since the upper layers impact the lower layers in the process. The ratio of last layer width to depth is shown in Fig. 6c. As the distance from the center increases, the width/depth ratio also increases. The effect of the location or incidence angle on the width and depth of the melt pool is considered statistically significant, and the corresponding probability value (p-value) calculated by the one-way analysis of variance (ANOVA) is less than the set significance level ($\alpha = 0.05$) [46,47].

Additionally, moving farther away from the center increased the surface roughness due to the loss of power density and hence weaker melting power. The top surface roughness of each specimen was measured using a Keyence VHX-1000 digital microscope. Fig. 6a shows the top surface map of a printed part. Four lines measurements (each line = 9.5 mm in length) were then taken from each surface map, and the arithmetic mean roughness values (Ra) were calculated for each line measurement. The average of mean values for the four lines were then calculated to obtain the final surface roughness. By analyzing the surface topographies, it was evident that the parts manufactured in the central location of the build plate had better surface quality than the parts located in the outer border of the platform (Fig. 6b).

4.3. Effect of orientation on the melt pool geometry and energy density

Table 3 shows the corresponding power and energy densities at different locations on the build plate. The specimen orientation can alter the energy density in the same location due to the change in the interaction time. Thus, one can compensate for the laser incidence angle and beam elongation effect by changing the orientation of the specimen in order to adjust the beam shape-dependent interaction time. The results from Fig. 7 show that different depths of penetration can be reached depending on the laser scan direction and laser incidence angle. The change in beam diameter causes the variance due to laser elongation, affecting the interaction time and power density (see Table 3). For instance, the second case in Table 3 shows a condition where the elongation of the laser beam and the laser scan direction are in parallel. In this condition, with constant speed and laser power, the power density decreases, and interaction time increases simultaneously hence keeping the energy density almost unaffected. In the third case, the elongation of a laser beam and the laser scan direction are perpendicular. Consequently, the melt pool depth decreases due to a lower energy density since the power density decreases while the interaction time remains the same.

In general, the outcome of using an elongated beam in a perpendicular (case 2) direction was a wider melt pool profile and not much change on the melt pool depth since the depth of the melt pool depends on the product of power density and the interaction time [44]. Therefore, in case 2, depth profiles similar to the center parts can be achieved as the energy densities in both cases are similar (Fig. 7). The extended interaction time due to the elongation can cancel the effect of the lower power density as a result of the increased area of the beam in the laser scan direction. Hence, similar energy densities result in similar penetration depths. Nevertheless, in the crosswise direction (case 3), the power density is decreased, but the interaction time remains constant with respect to the center specimen, resulting in reduced energy density and melt pool depths. However, the melt pool width increased in this case since it is mainly dependent on the laser beam diameter, which is elongated in the direction perpendicular to the scan direction. The concept of interaction time and power density could be used to develop a compensation algorithm to mitigate this effect which will be investigated in a future study.

Fig. 8 shows the quantitative plots of power, energy density, and interaction time variations based on Eqs. (1)–(3). As shown in Fig. 8a, the laser power density decreases as a function of the laser incidence angle regardless of the elongation direction as it only varies by the change in the laser spot area for a given power. However, as shown in Fig. 8b and c, the interaction time and energy density significantly change for elongations that are parallel or perpendicular to the scan direction. The interaction time stays constant when the elongation and scan directions are perpendicular (Fig. 8b), while it increases for the parallel case. Similarly, Fig. 8c shows the energy density variations for parallel and perpendicular cases. Since the energy density is the product of laser power density and interaction time, the energy density drops by decreasing the power density in a perpendicular case with a constant interaction time. However, increasing the interaction time in the parallel case compensates for the power density loss and keeps the energy density almost constant.

4.4. Effect of energy density distribution on the quality of the parts

To investigate the quality of parts in different locations and for different energy densities, 2D porosity distributions were imaged and analyzed at different cross-sectional areas (at least three distinct sections) for each specimen. The defect density of the parts in the center of the build plate was the least since the process parameters are typically

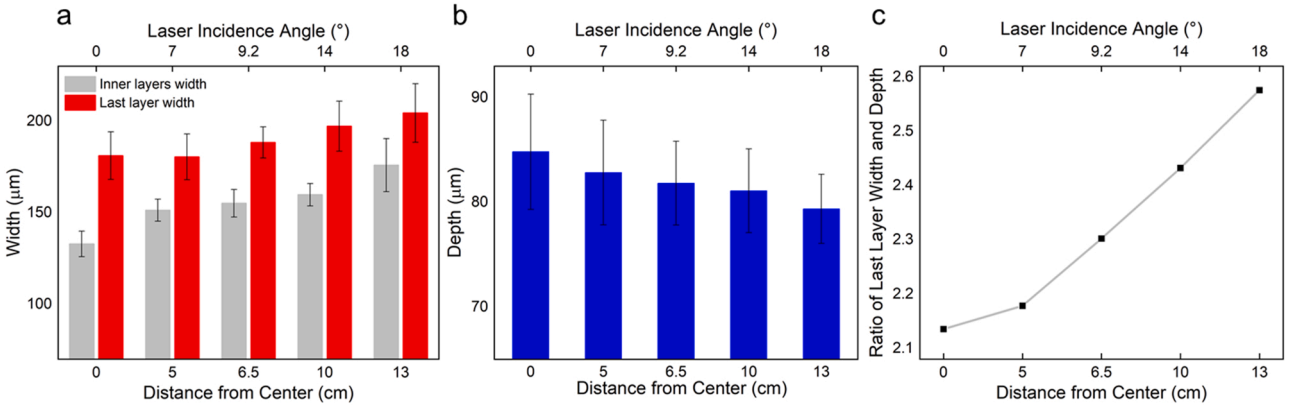

Fig. 5. Melt pool geometry versus distance from the center and incidence angle. The melt pool widths of inner layers and the last layer (a), melt pool depths of the last layer (b), and the ratio of last layer width to depth (c).

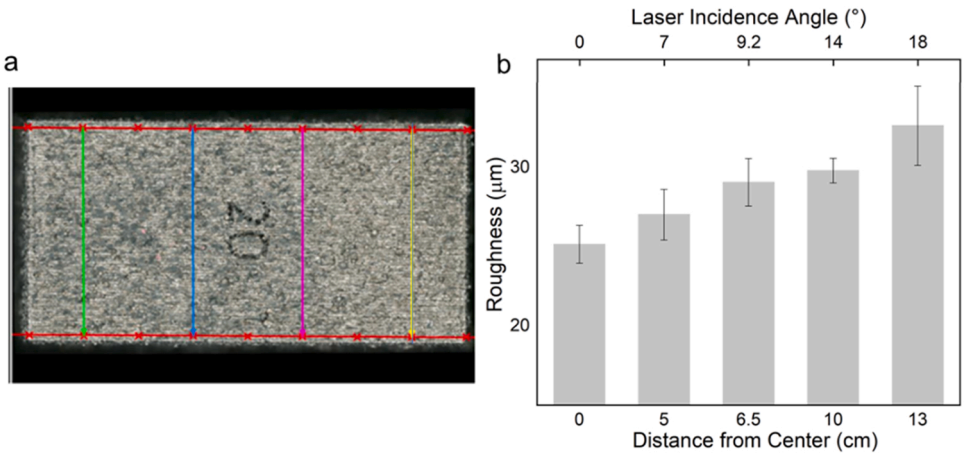

Fig. 6. Roughness results obtained by taking four line-profile measurements from of top surface of the samples (a). The mean values obtained from each sample (b) indicating a clear increase in the roughness as a function of distance from the center and laser incidence angle.

Table 3
Variation of power density, interaction time, and energy density depending on the laser incidence angle on the build plate for constant laser power and scan speed.

Case number	Distance from center (mm)	Laser incidence angle (°)	Beam length in elongation dir. (μm)	Beam length in scan dir. (μm)	Spot area (μm^2)	Power density (kW/mm^2)	Interaction time (μs)	Energy density (J/mm^2)
1	0	0	70.00	70.00	3846.50	51.99	132	6.86
2	100	14	72.14	72.14	3964.09	50.45	136	6.84
3	100	14	72.14	70.00	3964.09	50.45	132	6.65
4	130	18	73.59	71.20	4043.77	49.40	134	6.61

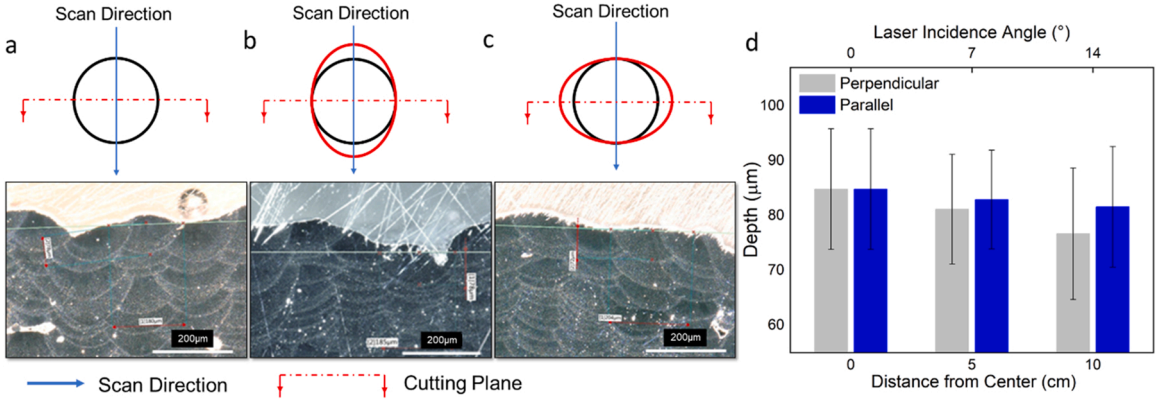

Fig. 7. Optical images of the microstructure with different orientation: central part (case 1) (a), 100 mm distance from the center (incidence angle 14°) when elongation and travel directions are parallel (case 2) (b), 100 mm distance from the center (incidence angle 14°) when elongation and laser scan direction are perpendicular (case 3) (c), and the melt pool depth of the last layer for both parallel (case 2) and perpendicular (case 3) cases (d).

optimized around the center. If the power and energy densities decrease from the optimum process parameters, it is expected to enter the lack of fusion or keyhole regimes in the process. Figs. 9 and 10 show the optical images of the defects for parts printed at different locations of the build plate and their corresponding pore size distribution, respectively. Figs. 9a and 10a show the results from a specimen at the center of the build plate with the least amount of defects as expected. If the interaction time did not change by getting farther from the center (as described earlier), the decreased power and energy densities due to the beam elongation effect cause more lack of fusion defects and porosity in the specimen, as shown in Figs. 9b,c and 10b,c. Comparing Figs. 9a,d and 10a,d, it can be observed that the energy densities are almost the same and hence providing similar porosity and defect levels. This is a promising observation that shows the potential of compensating for the unwanted beam elongation effects at different locations by controlling the specimen orientation. It is worth noting that since the used process parameters were the recommended parameters provided by the machine manufacturer (Renishaw), the energy density either reduces or stays the same as the beam moves away from the center. Thus, it is expected that most of the observed porosities are due to the lack of fusion. In addition, pores with irregular shapes in Fig. 9b and c seem to be lack of fusions, as reported in the literature [48,49].

The quantitative porosity values, plotted in Fig. 11, show energy density variation for different locations. As expected, this shows that the lower energy density can result in more porosity in the as-fabricated parts. This indicates that the energy density plays a considerable role in the formation of volumetric defects in the parts [50]. Designing process parameters that compensate for the changes in energy density will result in similar part quality and porosity levels at various locations. For instance, the specimens at the center (Fig. 9a) and 100 mm away (Fig. 9d) show almost the same porosity due to the energy density compensation effect.

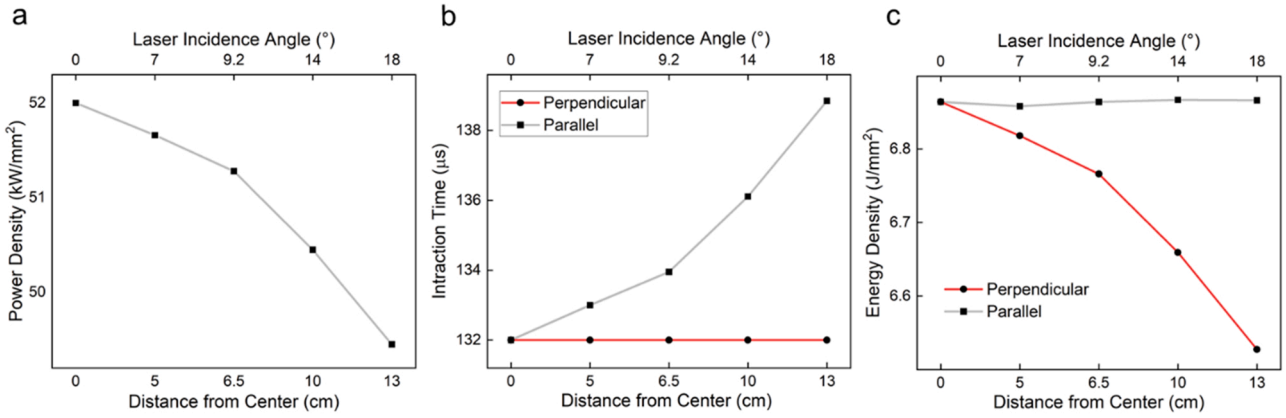

Fig. 8. Quantitative graphs of power density (a), interaction time (b), and energy density (c) variations based on Eqs. (1)–(3).

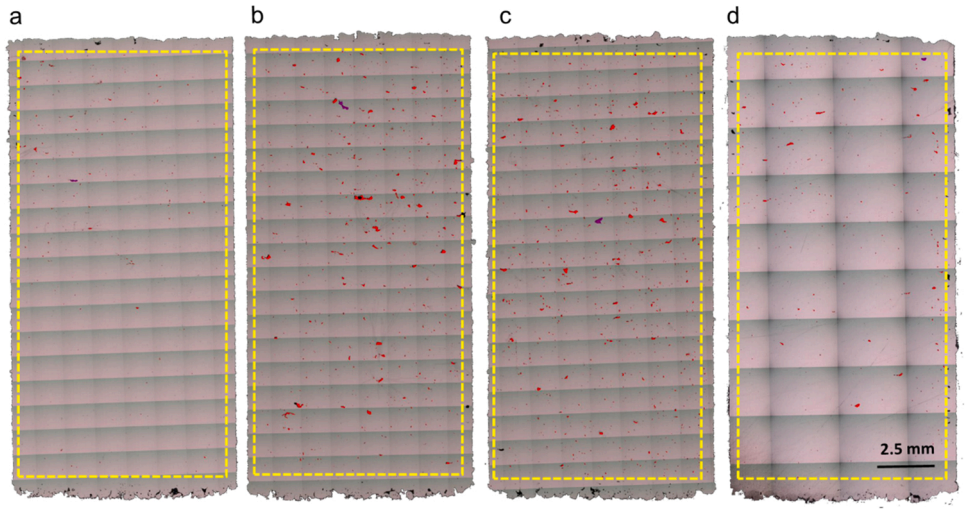

Fig. 9. 2D optical images of location-dependent porosity levels: 0 mm (incidence angle 0°) (case 1) (a), 100 mm (incidence angle 14°) (case 3) (b), 130 mm (incidence angle 18°) (case 4) (c), and 100 mm (incidence angle 14°) (case 2) (d).

5. Conclusion

In this study, the influence of laser incidence angle on the laser interaction cross-section across the build plate and the resulting impact on the melt pool profile, geometrical variations, power and energy density, porosity, and quality of parts were investigated.

1. It was found that the elongation of a laser beam indeed affected the resulting melt pool profile in the final parts. As the specimens were placed farther away from the center, the laser incidence angle increased from 0° at the center down to about 20° in the corners for the employed LB-PBF machine and build plate size in this study.
2. The laser interaction cross-section was circular at the center, and it became more elliptical in shape depending on the angle of incidence close to borders. The beam elongation increased the area of the interaction cross-section by up to 6.7% and hence decreased power density up to 6%. Accordingly, the width of the melt pools became wider, and their depths depended on the scan direction in correlation to the elongated direction.
3. For a constant interaction time, when elongation direction and scan direction were perpendicular, moving farther away from the center increased the spot area, and decreased the power and energy density, and hence decreased the depth of the melt pool. When the elongation and scan direction were parallel, the longer beam length increased the interaction time that compensated for energy loss due to the elongation. Therefore, the resulting melt pool exhibited a depth comparable to the circular beam at the center location.
4. The lack of fusion defects and surface roughness were prominent for parts manufactured with elongated beams, especially if the elongation direction was perpendicular to the scan direction.

In summary, this study provides a fundamental understanding of the possible sources of variations in the AM parts from a laser-materials interaction perspective. This will allow the manufacturer to design strategies such as dynamic tuning of the laser power, scan speed, and direction to compensate for such variation and manufacture uniform parts across the build plate.

CRediT authorship contribution statement

Parvin Fathi-Hafshejani: Conceptualization, Methodology, Validation, Formal analysis, Data curation, Investigation, Writing – original draft, Visualization. **Arash Soltani-Tehrani:** Conceptualization, Methodology, Validation, Writing – review & editing. **Nima Shamsaei:** Conceptualization, Methodology, Validation, Formal analysis, Resources, Data curation, Investigation, Writing – review & editing, Funding administration. **Masoud Mahjouri-Samani:** Conceptualization, Methodology, Resources, Formal analysis, Investigation, Writing – review & editing, Supervision, Project administration.

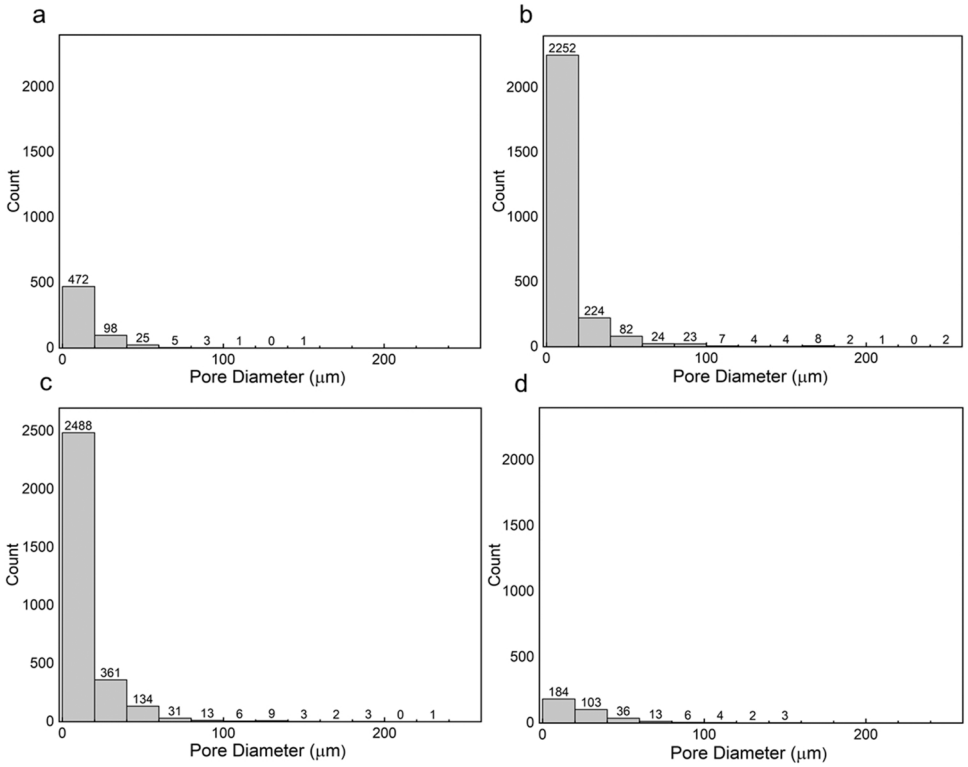

Fig. 10. A histogram representation of the effective pore diameter for part printed at different location of build plate: 0 mm (incidence angle 0°) (case 1) (a), 100 mm (incidence angle 14°) (case 3) (b), 130 mm (incidence angle 18°) (case 4) (c), and 100 mm (incidence angle 14°) (case 2) (d). These data are obtained from the samples shown in Fig. 8.

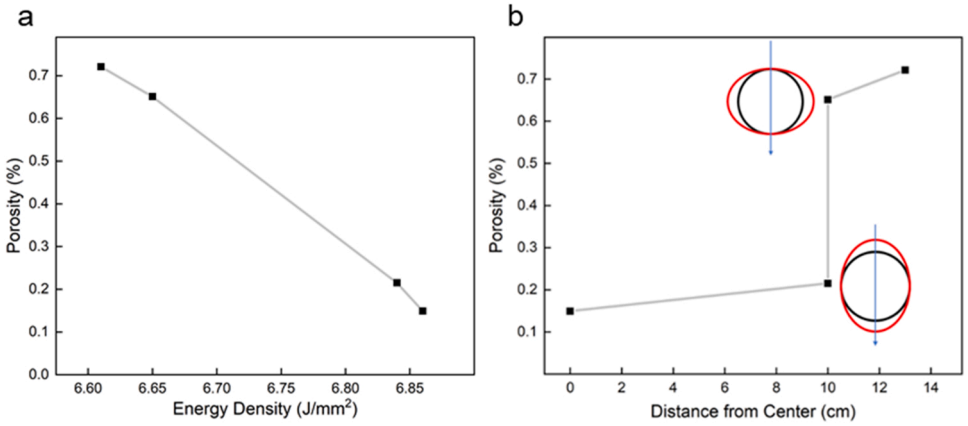

Fig. 11. Porosity values at different energy densities (a) and locations of the build plate (b). The elongated beam can produce similar porosity levels as the center part if the direction of the scan is in parallel to the elongations' direction, hence resulting in similar energy density levels.

Declaration of Competing Interest

The authors declare no conflict of interest.

Acknowledgments

This research was partially funded by the U.S. Federal Aviation Administration (FAA) under grant No. 12-C-AM-AU-003.

References

[1] Kik, T.J.M., Heat source models in numerical simulations of laser welding. 2020. 13(11): p. 2653.
[2] P. Fathi-Hafshejani, H. Johnson, Z. Ahmadi, M. Roach, N. Shamsaei, M. Mahjouri-Samani, Phase-Selective and Localized TiO2 Coating on Additive and Wrought Titanium by a Direct Laser Surface Modification Approach, Phase-Selective and Localized TiO2 Coating on Additive and Wrought Titanium by a Direct Laser Surface Modification Approach. 2020. 5(27): p. 16744–16751.
[3] T. Zhang, et al., Effect of laser remelting on microstructural evolution and mechanical properties of Ti-35Nb-2Ta-3Zr alloy, Mater. Lett. 253 (2019) 310–313.
[4] A. Temmler, N.J.A.S.S. Pirch, Investigation on the mechanism of surface structure formation during laser remelting with modulated laser power on tool steel H11, Appl. Surf. Sci. 526 (2020), 146393.
[5] A. Wetzig, et al., Fast laser cutting of thin metal, Proc. Manuf. 29 (2019) 369–374.
[6] S. Guarino, et al., Environmental assessment of Selective Laser Melting compared with Laser Cutting of 316L stainless steel: a case study for flat washers' production, CIRP J. Manuf. Sci. Technol. 31 (2020) 525–538.
[7] M. Landowski, et al., Autogenous fiber laser welding of 316L austenitic and 2304 lean duplex stainless steels, Materials 13 (13) (2020) 2930.
[8] M. Sahul, et al., Effect of disk laser beam offset on the microstructure and mechanical properties of copper—AISI 304 stainless steel dissimilar metals joints, Met. Open Access Metall. J. 10 (10) (2020) 1294.
[9] Vilar, R.J.Jola, Laser cladding. 1999. 11(2): p. 64–79.

[10] A.A. Siddiqui, A.K.J.O. Dubey, L. Technology, Recent trends in laser cladding and surface alloying, Opt. Laser Technol. 134 (2021), 106619.
[11] P. Fathi-Hafshejani, et al., Laser-assisted selective and localized surface transformation of titanium to anatase, rutile, and mixed phase nanostructures, J. Laser Appl. 33 (1) (2021), 012014.
[12] M. Gong, et al., Laser-arc hybrid additive manufacturing of stainless steel with beam oscillation, Addit. Manuf. 33 (2020), 101180.
[13] Y. Liu, Y.J.M.S. Zhang, E. A, Microstructure and mechanical properties of TA15-Ti2AlNb bimetallic structures by laser additive manufacturing, Mater. Sci. Eng. A 795 (2020), 140019.
[14] R. Russell, et al., Qualification and certification of metal additive manufactured hardware for aerospace applications*, Addit. Manuf. Aerosp. Ind. (2019) 33–66.
[15] G. Strano, et al., Surface roughness analysis, modelling and prediction in selective laser melting, J. Mater. Process. Technol. 213 (4) (2013) 589–597.
[16] B.-Q. Li, et al., Research on surface roughness of AlSi10Mg parts fabricated by laser powder bed fusion, Met. Open Access Metall. J. 8 (7) (2018) 524.
[17] K. Mumtaz, N.J.R.P.J. Hopkinson, Top surface and side roughness of Inconel 625 Parts processed using selective laser melting, Rapid Prototyp. J. (2009).
[18] A. Leon, E.J.M.C. Aghion, Effect of surface roughness on corrosion fatigue performance of AlSi10Mg alloy produced by Selective Laser Melting (SLM), Mat. Character. 131 (2017) 188–194.
[19] F. Bosio, et al., A time-saving and cost-effective method to process alloys by Laser Powder Bed Fusion, Mater. Des. 181 (2019), 107949.
[20] A. Rahmani, A.-H.I. Mourad, On the use of additive manufacturing for mechanical performance assessment of engineering materials: a review. in 2020 Advances in Science and Engineering Technology International Conferences (ASET). IEEE.
[21] K.V. Wong, , A.J. Isrn Hernandez, A review of additive manufacturing, 2012.
[22] W.E.J.Jo.M.E. and performance, Metal additive manufacturing: a review. 2014. 23 (6): p. 1917–1928.
[23] B. Foster, et al. Optical, layerwise monitoring of powder bed fusion. in Solid Freeform Fabrication Symposium, Austin, TX, Aug. 2015.
[24] L. Dowling, et al., A review of critical repeatability and reproducibility issues in powder bed fusion, Mater. Des. 186 (2020), 108346.
[25] E. Santecchia, S. Spigarelli, M.J.M. Cabibbo, Material reuse in laser powder bed fusion: Side effects of the laser—metal powder interaction, Met. Open Access Metall. 10 (3) (2020) 341.
[26] T.T. Roehling, et al., Modulating laser intensity profile ellipticity for microstructural control during metal additive manufacturing, Acta Mater. 128 (2017) 197–206.
[27] E.J.A.M. Soylemez, High deposition rate approach of selective laser melting through defocused single bead experiments and thermal finite element analysis for Ti-6Al-4V, Addit. Manuf. 31 (2020), 100984.
[28] T. Zhang, et al., Evolution of molten pool during selective laser melting of Ti-6Al-4V, J. Phys. D Appl. 52 (5) (2018), 055302.
[29] J.C. Heigel, B.M. Lane, Engineering, Measurement of the melt pool length during single scan tracks in a commercial laser powder bed fusion process, J. Manuf. Sci. Eng. 140 (2018) 5.
[30] J. Pegues, et al., Fatigue of additive manufactured Ti-6Al-4V, Part I: the effects of powder feedstock, manufacturing, and post-process conditions on the resulting microstructure and defects, Int. J. Fatigue 132 (2020), 105358.
[31] Z. Ahmadi, et al., Rapid laser nanomanufacturing and direct patterning of 2D materials on flexible substrates-2DFlex, Nanotechnology 32 (5) (2020), 055302.
[32] R. Molaei, et al., Fatigue of additive manufactured Ti-6Al-4V, part II: the relationship between microstructure, material cyclic properties, and component performance, Int. J. Fatigue 132 (2020), 105363.
[33] Z. Ahmadi, P. Fathi-Hafshejani , M. Mahjouri-Samani . Laser patterning and crystallization of 2D materials on rigid and flexible substrates. in Synthesis and Photonics of Nanoscale Materials XVIII. 2021. International Society for Optics and Photonics.
[34] S. Kleszczynski, et al. Position dependency of surface roughness in parts from laser beam melting systems. in 26th Internation Solid Free Form Fabrication (SFF) Symposium, Austin, TX, Aug. 2015.
[35] S. Sendino, et al., The effect of the laser incidence angle in the surface of L-PBF processed parts, Coatings 10 (11) (2020) 1024.
[36] A., Soltani-Tehrani, , J. Pegues, N.J.A.M. Shamsaei, Fatigue behavior of additively manufactured 17–4 PH stainless steel: the effects of part location and powder re-use. 2020. 36: p. 101398.
[37] T. Fiegl, et al., Impact of build envelope on the properties of additive manufactured parts from AlSi10Mg, Opt. Laser Technol. 111 (2019) 51–57.
[38] S. Rott, et al., Surface roughness in laser powder bed fusion – Interdependency of surface orientation and laser incidence, Addit. Manuf. 36 (2020), 101437.
[39] J. Pegues, et al., Surface roughness effects on the fatigue strength of additively manufactured Ti-6Al-4V, Int. J. Fatigue 116 (2018) 543–552.
[40] W. Ayoola, et al., Effect of beam shape and spatial energy distribution on weld bead geometry in conduction welding, Opt. Laser Technol. 117 (2019) 280–287.
[41] W. Suder, S.J.Jola Williams, Investigation of the effects of basic laser material interaction parameters in laser welding, J. Laser Appl. 24 (3) (2012), 032009.
[42] West, B., R. Russell, D. Wells, NASA's Approach to Additive Manufacturing Certification: Methodologies for Qualification of Additively Manufactured Aerospace Hardware. 2019.
[43] J. Tan, C. Tang, C.J.M.C. Wong, Study and modeling of melt pool evolution in selective laser melting process of SS316L, MRS Commun. 8 (3) (2018) 1178–1183.
[44] G. Tapia, et al., Gaussian process-based surrogate modeling framework for process planning in laser powder-bed fusion additive manufacturing of 316L stainless steel, Int. J. Adv. Manuf. Technol. 94 (9) (2018) 3591–3603.
[45] Y. Tian, et al., Melt pool morphology and surface roughness relationship for direct metal laser solidification of Hastelloy X, Rapid Prototyp. J. (2020).
[46] D.C. Montgomery, G.C. Runger, Applied Statistics and Probability for Engineers, John Wiley & Sons, 2010.
[47] D.C. Montgomery, Design and Analysis of Experiments, John Wiley & Sons, 2017.
[48] N. Emminghaus, et al., Residual oxygen content and powder recycling: effects on surface roughness and porosity of additively manufactured Ti-6Al-4V, Addit. Manuf. 4V (2021), 102093.
[49] T. Vilaro, et al., As-fabricated and heat-treated microstructures of the Ti-6Al-4V alloy processed by selective laser melting, Metallur. Mater. Trans. 42 (10) (2011) 3190–3199.
[50] A. Soltani-Tehrani, et al., Establishing specimen property to part performance relationships for laser beam powder bed fusion additive manufacturing, Int. J. Fatigue (2021), 106384.